Network-Aided Pseudorange-Based LEO PNT from OneWeb

Zacharias M. Komodromos*, Samuel C. Morgan†, Zachary L. Clements†, Wenkai Qin†, W. Jeremy Morrison†, Todd E. Humphreys†

*Department of Electrical and Computer Engineering, The University of Texas at Austin

†Department of Aerospace Engineering and Engineering Mechanics, The University of Texas at Austin

***Abstract*—This paper presents a framework and first experimental results for pseudorange-based positioning, navigation, and timing (PNT) exploiting OneWeb's Ku-band downlink signal and a reference network. As the demand for accurate and resilient positioning and timing solutions grows, the proliferation of low Earth orbit (LEO) satellites, including approximately 650 in OneWeb's constellation, offers promising opportunities for powerful new PNT services. Newly discovered synchronization sequences embedded in the OneWeb signal open the way for third-party provision of highly accurate clock and orbital models for each OneWeb satellite. Model parameters would be continually estimated by a sparse network of reference stations at known locations having access to an accurate universal time scale such as UTC. Subscribers to the third party's data feed could treat OneWeb much like a traditional GNSS, extracting pseudorange, carrier phase, and Doppler observables directly from the OneWeb signals, either by exploiting only the newly discovered synchronization sequences or augmenting these with additional sequences decoded continuously by the reference network. The observables would then be processed together with the third-party-provided models to produce highly accurate position, velocity, and timing solutions. Because each OneWeb satellite illuminates a wide geographic area, this technique could be implemented with an attractively low density of reference stations. In this paper we develop the OneWeb satellite clock model, establish its applicability across multiple downlink beams, analyze the effect of ephemeris errors on the resulting solution, and prove the technique in a field experiment with live signals, achieving sub-meter-level positioning and timing.**

***Index Terms*—OneWeb, signal processing, positioning, low Earth orbit, CDGNSS.**

I. Introduction

Dual purposing broadband communication signals from low Earth orbit (LEO) mega-constellations for positioning, navigation, and timing (PNT) is the subject of a rapidly growing body of research [1]–[6]. LEO signals potentially offer more robust, secure, and accurate PNT compared to traditional Global Navigation Satellite System (GNSS) signals due to their significantly larger bandwidth, higher received power, superior geometric diversity, and larger constellation size [1]. Thus, they could be the basis of a PNT service that acts as a complement to or a backup for traditional GNSS amid rising threats of GNSS jamming and spoofing [7]–[11]. OneWeb's Ku-band downlink signal exemplifies the capabilities of LEO signals used for broadband communication, providing 230 MHz-wide channels from around 650 satellites that are 15 times closer to Earth than traditional GNSS satellites [12]. OneWeb's polar orbits offer global coverage, and their space-to-Earth link operates in the reasonably accessible 10.7—12.7 GHz band.

The great majority of opportunistic LEO PNT methods presented in the literature are Doppler-based [13]. But compared to pseudorange-based PNT techniques, Doppler-based techniques have worse timing accuracy by many orders of magnitude (milliseconds vs. nanoseconds), even under optimistic measurement noise and satellite clock offset rate assumptions [4], [14], [15]. Recognizing that many PNT applications of practical interest require accurate timing, we focus on pseudorange-based PNT, or PNT based on time-of-arrival (TOA) measurements.

The extraordinary bandwidth of the OneWeb signal is a boon for TOA measurements, providing far more resistance to multipath than the widest traditional GNSS signal, the 51.15-MHz Galileo E5 AltBOC signal. Moreover, the OneWeb signal does not suffer from the side-peak ambiguity problem inherent in Galileo AltBOC processing [16].

The approach proposed in this paper leverages pseudorange measurements for a navigation solution and uses signals from OneWeb's constellation. Any method relying on pseudorange measurements is limited by the clocks at the receiver and the satellite. As recent work indicates, clocks onboard LEO satellites meant for broadband communication may not meet the stringent requirements of PNT applications [17], [18]. To counteract any timing errors, two receivers can be used to cooperatively form the PNT solution. In this framework, a reference station (RS) can act as a reference receiver with a known position and reliable timing. While OneWeb's satellites move overhead, the RS can estimate the transmission time of a frame, the channel it was transmitted on, and estimate clock errors. The second receiver, the user equipment (UE), can use this information to form TOA measurements with reduced effects from the satellite's clock errors. In low signal-to-noise (SNR) ratio regimes, the RS could provide more payload symbols to extend the integration period used to collect TOA measurements. The UE could be consumer-grade hardware with an omnidirectional antenna and a lower-quality clock. Especially with the plethora of reasonably priced feedhorn and low noise blocks (LNBs) for Ku-band due to their mass production, the UE need not be expensive.

This TOA-based approach would require the signal structure to be known, which is a challenge for LEO signals like that of OneWeb since their signals are not standardized, nor designed

Preprint of the 2025 IEEE/ION Position, Location, and Navigation Symposium (PLANS), Salt Lake City, UT, April 28-May 1, 2025

for navigation [19]. Progress has been made with Starlink's signal structure with the discovery of synchronization sequences that unlock the potential for pseudorange-based PNT [5]. The soon-to-be published work on which this paper relies uncovers details about OneWeb's signal [20]. Perhaps the most significant discovery is a short synchronization sequence that repeats every 1 ms, which unlocks pseudorange-based PNT with OneWeb.

Our proposed framework assumes the RS can communicate timing corrections and payload information to the UE within a reasonable time frame. The information an RS communicates becomes stale as different satellites pass overhead, or as a single satellite's clock drifts. The minimum refresh interval for the clock model is the duration a single beam illuminates the same area, but could possibly be longer if the beams depend on the same clock. Since OneWeb's satellites have a fixed beam pattern consisting of 16 beams, a study must be conducted to determine if clock corrections for one beam can be used for the entire satellite footprint. A contribution of this paper is evidence that beam-to-beam clock consistency of a single satellite is consistent enough that the clock corrections from the RS could be used for PNT within at least one beam footprint, which is conservatively around 67×1080 km^2.

A. Related Work

Four strategies for realizing LEO PNT are summarized in Table I. The first is a dedicated approach, where satellites from companies like Xona Systems and TrustPoint have a dedicated PNT mission with high deployment cost. The second is a fused approach, in which broadband LEO communications SVs also offer a communications service, which comes at the cost of some lost communication capacity [1], [6], [23], [24], [29]. Both of these approaches offer high accuracy, but at a cost assumed by the constellation owner.

This paper explores the third strategy, in which a network of reference stations provides corrections to pseudorange, Doppler, or carrier-phase measurements of existing LEO satellite signals. In the simplest embodiment, the network is a single reference station. Previous studies rely on Doppler measurements [26], or have only considered pseudorange measurements from OneWeb in simulation [27]. Authors in [28] conducted a study similar to this paper's using Iridium's signal and achieved impressive results, considering the comparatively smaller bandwidth.

Note that Table I also classifies the opportunistic approach presented in [25] as network-aided because the receiver being tracked is aided by GNSS signals during an initialization phase, which allows estimation of LEO satellite ephemeris, clock, and clock rate errors just as occurs with network aiding. In effect, the receiver acts as its own reference station during the initialization phase, holding over key estimated values during the GNSS-denied phase.

The fourth strategy in Table I is the stand-alone opportunistic approach, where unmodified LEO constellations are exploited for PNT using only publicly available data and no network aiding.

The first two strategies rely on cooperation with the constellation owner and are not the focus of this paper. The stand-alone opportunistic approach has not been demonstrated to offer accuracy competitive with traditional GNSS. Recent results in [18] indicate that stand-alone opportunistic use of Starlink for pseudorange-based PNT would fail to offer solutions remotely competitive with traditional GNSS due to satellite timing peculiarities that appear impossible to model. This is also likely true for OneWeb, though a study like [18] has yet to be done for OneWeb. Thus, a network-aided opportunistic approach remains a promising strategy for realizing LEO PNT, since a third-party's network would provide measurement corrections, obviating the need for a model of mercurial satellite clock variations. As more becomes known about OneWeb's signal, and additional synchronization sequences are discovered, the network-aided opportunistic approach could become even more attractive.

B. Contributions

This paper outlines the framework in which an RS could provide information to UE located within the same satellite beam footprint, enabling PNT. We offer 3 contributions. First, we develop the necessary clock model that an RS would need to provide to a UE. Second, we study the effects of ephemeris errors on the final positioning solution, and study the effect on the TOA RMSE of sharing more payload symbols with the UE. Third, we conduct a field experiment with live signals to demonstrate the feasibility of the framework, achieving a sub-meter final solution error. The success of this framework could motivate a third party to provide PNT services using OneWeb's Ku-band downlink signal, or could provide an example for fused GNSS for the constellation's owners.

II. Concept of Operations

Suppose a third party wants to provide PNT services using OneWeb's Ku-band downlink signal. They can commission a stationary RS at a known location, with a good quality clock, prior knowledge of the satellite ephemerides, and a communication link for any UE subscribed to their service, as depicted in Fig. 1. The RS clock could be disciplined to GNSS or alternatively, for a GNSS-independent approach, the third party might utilize atomic clocks or time signals from other terrestrial broadcast systems for RS clock disciplining. Additionally, the RS boasts a high gain Ku-band antenna to capture the downlink signal and extract the payload.

OneWeb's roughly 650 satellites follow polar orbits at an altitude of 1200 km. Their downlink signal has approval for the 10.7–12.7 GHz space-to-Earth frequency band. Each channel supports a $F_{\text{sym}} = 230.4$-MHz wide single-carrier Time Division Multiple Access (SC-TDMA) signal, with frames being transmitted every $T_{\text{f}} = 10$ ms [20]. Assuming OneWeb is transmitting a QPSK signal, the RS could easily demodulate frames and re-broadcast the data as an uncompressed constant stream of 57.6 MB/s if every symbol of every frame is required - a rate which would be cost ineffective. Furthermore, using the known position of the RS and the satellite, the RS could provide the time of transmission (TOT) for each frame, with some correction for the satellite's clock error.

TABLE I: LEO PNT Strategies

	Dedicated [19], [21], [22]	Fused [1], [6], [23], [24]	Network-Aided Opportunistic [25]–[29]	Stand-Alone Opportunistic [4], [14], [30]–[32]
Description	LEO constellation or hosted payloads dedicated solely to PNT.	Fuses a secondary PNT service with a primary communications service.	Like stand-alone opportunistic, but a network of reference stations provides corrections.	Exploits unmodified signals from communications SVs. Public ephemerides. No network aiding.
Marginal deployment cost	high: constellation of SVs	low: uses communications hardware and signals	high: network of reference stations	very low
Potential availability	mid-term	near-term	near-term for local coverage	immediate
Potential accuracy [m]	< 1	< 1	< 1	< 100
Time to fix [s]	< 10	< 10	< 10	< 1000
Dependency on traditional GNSS	@SVs in near-term	@SVs in near-term	@reference stations in near-term	@SVs in some cases

The RS would serve consumer-grade UE with a lower quality clock and an omnidirectional Ku-band antenna. Using the RS's broadcasted data, the UE could form TOA measurements using local replicas from the RS decoded payload. These TOAs with the clock corrected TOTs form pseudorange measurements that the UE can use to estimate its position and clock error.

Before such a framework is implemented, certain challenges must be addressed. The first challenge is that of the SV clock error and stability, where these effects could act much like the clock dithering implemented to intentionally degrade GPS accuracy under the Selective Availability program discontinued in May 2000 [33]. The second challenge is determining the refresh rate of the clock models, and the payload information, since the maximum 57.6 MB/s is a costly burden to meet in real-time. The third challenge is the effect of ephemeris errors on the final positioning solution, since a third-party may not have access to the more precise satellite ephemerides required for collision avoidance.

All these questions are intrinsically linked to the signal structure of OneWeb's signal, their fixed beam pattern, and polar orbits. Given their constellation, only a beam from a single satellite illuminates a receiver at a given time. From the satellite's 16 beams, only 8 are active per channel with roughly 20 seconds between the apex in power of each beam [20].

In this paper we will address the above challenges and provide an experimental demonstration of the framework using at most 4 of the 8 active beams per satellite. Due to our experimental setup, the TOA measurements could not be obtained in quick succession, but rather in bursts with small gaps between the beams, and larger gaps when switching between satellites. This increases the burden on our UE to estimate its clock bias and bias rate during the gaps, as its own clock drifts.

III. Signal Model

OneWeb employs a Multi-Frequency Time Division Multiple Access (MF-TDMA) Single Carrier (SC) scheme, on each of 8 separate frequency channels [20]. Only three channels, centered at 11.075, 11.325, and 11.575 GHz are presently active over our location in Austin, Texas. Each channel is modulated with a QPSK signal, although documentation for their user terminal (UT) suggests support for QPSK, 8PSK, and 16APSK [34].

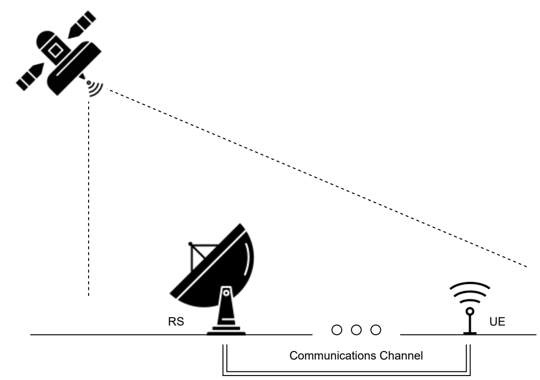

Fig. 1: Diagram of the proposed framework. A network of reference stations (RSs) provides timing and ephemeris corrections along with data payload symbols to user equipment (UE) through a side channel. The UE then gathers TOA measurements using the RS-broadcasted payload data and forms pseudorange measurements with the provided TOTs.

A. QPSK Signal Model

Fundamentally, a SC signal is a train of pulses, each modulated by a phase and amplitude shift corresponding to the data symbol being transmitted on that pulse. The resulting continuous stream of symbols can be characterized by a simple signal model. The baseband signal model for a SC QPSK signal is given by

$$s(t) = \sum_{m} \exp(j\pi a_m/2) p\left(\frac{t - mT_{\text{sym}}}{T_{\text{sym}}}\right) \tag{1}$$

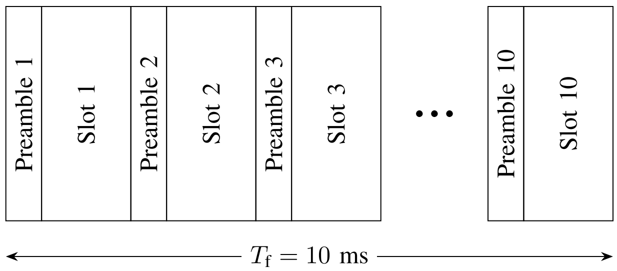

Fig. 2: Theorized frame structure of OneWeb's downlink signal.

where statistically independent symbol phases $a_m \in \{0, 1, 2, 3\}, m \in \mathbb{Z}$ can be encoded to represent two bits per symbol, and T_{sym} is the symbol period. Following the analysis from [20], $T_{\text{sym}} = 1/230.4\text{MHz}$, and $p(t)$ is the square root raised cosine (SRRC) pulse with a rolloff factor $\beta_r = 0.1$.

B. OneWeb Signal Structure

OneWeb's signal structure remains largely unknown. Over our location in Austin Texas, we have observed that satellite beam transmits a frame every $T_{\mathrm{f}} = 10$ ms. Our current hypothesis is that a frame consists of 10 slots, each with a preamble. Within the preamble exists a synchronization sequence which is common across all preambles. The payload data for each slot should contain unique data for each frame, but remains the same in the case the slot has not been assigned to a user. Fig. 2 is not to scale, as the preamble only lasts about 25 μs. The synchronization sequence, which lasts only 400 symbols [20], is a poor choice for a ranging sequence even though it is identical across all beams and satellites.

Our current observation is that the payload data used when the slot is not assigned to a user remains the same across frames from the same beam. Thus, as things stand, we need only decode a single 10-ms frame from each beam to accommodate TOA measurements for the entire duration the beam illuminates a receiver.

A stationary receiver can easily distinguish specific intervals corresponding to captures from different beams. Let such an interval be called a beam interval (BI). Given OneWeb only uses half of the 16 beams at a time, the BI can be as long as 20 seconds. A continuous capture of seven BIs from OneWeb-0114 on March 2024 is shown in Fig. 3, where a receiver can easily distinguish the different beams simply by using the received power. For the purposes of this paper, we chose to focus on 12-second BIs centered at the apex of transmitted power to ensure no interference in the data collection and maximize the number of symbols we can reliably decode. These manifest as the colored portions in Fig. 3. The use of 12-second BIs introduces a small 8-second gap between the end of one BI and the beginning of the next.

IV. Timing

Clocks onboard LEO satellites are of unknown quality, and may exhibit peculiarities as was recently revealed for Starlink's satellites [17], [18]. The clock model we develop in this section is necessary for the RS to provide timing corrections to the UE.

A. Transmitter Clock Model

We speculate that each satellite must have a base oscillator, probably disciplined to GNSS, that feeds a frame clock and a carrier clock for each beam. It may be that the beams use the same frame and carrier clocks, but this is still under investigation. Let t_{d} be the GNSS-disciplined timing signal that drives the frame clock timing signal t_{f} and the carrier clock timing signal t_{c}. The carrier clock is likely transparent, with $t_{\mathrm{c}} = t_{\mathrm{d}}$, while the frame clock depends on how baseband frames are loaded into buffers for mixing to the carrier frequency before transmission. Each of the two clocks may have offsets from t_{d} denoted as Δt_{f} and Δt_{c} respectively such that

$$t_{\mathrm{d}}(t) = t_{\mathrm{f}}(t) - \Delta t_{\mathrm{f}}(t) \tag{2}$$
$$t_{\mathrm{d}}(t) = t_{\mathrm{c}}(t) - \Delta t_{\mathrm{c}}(t) \tag{3}$$

where t represents true time. Each of these is thus related to true time by

$$t = t_{\mathrm{f}}(t) - \delta t_{\mathrm{f}}(t) \tag{4}$$
$$t = t_{\mathrm{c}}(t) - \delta t_{\mathrm{c}}(t) \tag{5}$$

where $\delta t_{\mathrm{f}}(t)$ and $\delta t_{\mathrm{c}}(t)$ are the frame and carrier clock offsets. This distinction is necessary to inform our estimation process later on, since pseudorange measurements would be affected by the frame clock and Doppler measurements by the carrier clock.

B. Discrete-Time Frame clock

Within a BI, frames arrive at a cadence of 10 ms. The first frame of a BI is somewhat arbitrary, especially in the case of a 12-second BI, since there is no clear feature indicating a first unique frame in a BI. Starting from the first observed frame in a BI, we can index the frames from 0 to $N_a - 1$ where $N_a = 1200$ for a 12-second BI.

Let $t_f(l, m)$ be the frame clock time at the time of transmission of the mth frame in the lth BI, where m and l are zero-indexed. This quantity is defined as

$$t_{\mathrm{f}}(l, m) \triangleq t(l) + mT_{\mathrm{f}} \tag{6}$$

where $t(l)$ is the time of the first frame in the lth BI. Let $t^*(l, m)$ and $\delta t_{\mathrm{f}}(l, m)$ be the corresponding GPS time (GPST) and frame clock offset. Then

$$t^*(l, m) = t_{\mathrm{f}}(l, m) - \delta t_{\mathrm{f}}(l, m) \tag{7}$$

The receiver clock offset $\delta t_{\mathrm{r}}(t_{\mathrm{r}})$ is represented as a function of t_{r} because it is natively ordered in receiver time in the course of solving for a position and time solution. The time derivative of δt_{r} with respect to t, denoted $\dot{\delta t}_{\mathrm{r}}(t_{\mathrm{r}}(t))$, is called the receiver clock drift.

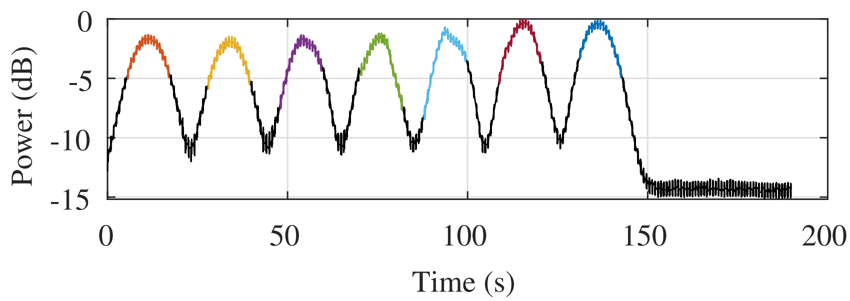

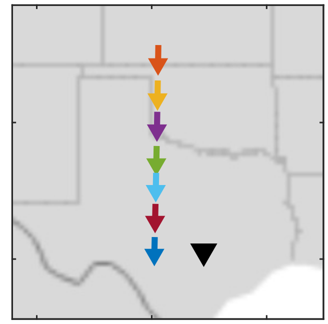

Fig. 3: Normalized power of the signal (left), with the associated ground track (right) of each BI and the receiver (marked by the triangle). Data are for ONEWEB-0114 from a capture centered at F_{c2} taken in March 2024.

Let $t_r(l,m)$ be the time of reception, according to the receiver clock, of the frame transmitted at true time $t^*(l,m)$. Let $\delta t_r(l,m)$ be the corresponding receiver clock offset and $t_*(l,m)$ be the corresponding true time of reception. More precisely, $t_r(l,m)$ is the receiver clock time at which the frame transmitted at true time $t^*(l,m)$ from the satellite's downlink antenna's phase center first reached the receiver antenna's phase center. The receipt time $t_r(l,m)$ can be related to $t_*(l,m), t^*(l,m)$, and $t_f(l,m)$ by

$$t_*(l,m) = t_r(l,m) - \delta t_r(l,m) \tag{8}$$

$$t^*(l,m) = t_r(l,m) - \delta t_r(l,m) - \delta t_{\text{tof}}(l,m) \tag{9}$$

$$t_f(l,m) = t_r(l,m) - \delta t_r(l,m) - \delta t_{\text{tof}}(l,m) + \delta t_f(l,m) \tag{10}$$

where $\delta t_{\text{tof}}(l,m)$ is the frame's time of flight from transmission to reception, expressed as an interval in true time.

C. Timing corrections

TOT calculation on the RS begins with the frame TOA measurement in receiver time. We subtract from this an estimate of the offset $\delta t_r(l,m)$ obtained from the simultaneously captured GNSS signals, accounting for the difference in length of the cables from our capture equipment to the GNSS and Ku-Band antennas. This process allows us to determine $t_*(l,m)$ to within a few ns, which, in turn, is related to $t^*(l,m)$ by

$$t^*(l,m) = t_*(l,m) - \delta t_{\text{tof}}(l,m) \tag{11}$$

What remains is to calculate the frame's time of flight, $\delta t_{\text{tof}}(l,m)$, modeled as

$$\delta t_{\text{tof}}(l,m) = \frac{1}{c} \cdot \|\boldsymbol{r}_r - \boldsymbol{r}_t(t^*(l,m))\| + \delta t_{\text{atm}} \tag{12}$$

where $\boldsymbol{r}_r$ is the receiver's location, $\boldsymbol{r}_t(t^*(l,m))$ is the transmitter's location at the TOT, and δt_{atm} is the atmospheric (neutral and ionospheric) delay experienced by the signal over its path from transmitter to receiver. Substituting (11) into (12) yields the implicit relationship

$$\delta t_{\text{tof}}(l,m) = \frac{1}{c} \cdot \|\boldsymbol{r}_r - \boldsymbol{r}_t(t_*(l,m) - \delta t_{\text{tof}}(l,m))\| + \delta t_{\text{atm}} \tag{13}$$

from which $\delta t_{\text{tof}}(l,m)$ can readily be calculated numerically, provided δt_{atm} and a smooth transmitter location function $\boldsymbol{r}_t(t)$.

To support determination of $t^*(l,m)$ to the best of our ability, errors in $\boldsymbol{r}_t(t)$, $\boldsymbol{r}_r$, and δt_{atm} must be small relative to this amount. For δt_{atm}, a Saastamoinen [35] neutral atmospheric model with average surface parameters was applied with Niell wet and dry mapping functions [36]; ionospheric delays, which are minimal at Ku-band, were ignored. The process is identical to that outlined in [18, Sec. VII-A].

Unlike the work in [18], we did not have access to meter-level accurate ephemerides for the satellites. Instead, we used the Two-Line Element (TLE) data provided by the North American Aerospace Defense Command (NORAD) to estimate the satellite's position at the time of transmission. This introduces an error in the $\delta t_{\text{tof}}(l,m)$ calculation, which we will address in Sec. VI.

V. Data Aiding

Given the SS for OneWeb is short, a high-gain antenna is required to extract TOA measurements accurately. Since the UE is assumed to be consumer-grade hardware, we must rely on the RS to provide the UE with additional symbols to extend the coherent integration period. This raises the questions of how much data the RS should provide, and how often.

A. Data burst duration

The duration of the data bursts directly impacts the quality of the TOA measurements the UE can obtain. This has been studied extensively in the literature [37], [38], and has been applied to Starlink's signal to provide RMSE bounds on the TOA measurements obtained from their signal [18]. The analysis for OneWeb is no different.

In short, the TOA error variance for a signal with Fourier transform $S(f)$ and post integration SNR E/N_0 can be expressed in the form [39, Eq. 11.15]

$$\sigma_\tau^2 \geq \frac{1}{2\gamma^2 \frac{E}{N_0}} \tag{14}$$

where γ^2 is the effective squared bandwidth defined as

$$\gamma^2 \triangleq \frac{\int_{-\infty}^{\infty} (2\pi f)^2 |S(f)|^2 df}{\int_{-\infty}^{\infty} |S(f)|^2 df}. \tag{15}$$

In Sec. VIII-B, we provide information on the UE setup which is limited to only 25 MHz of the 230.4 MHz wide

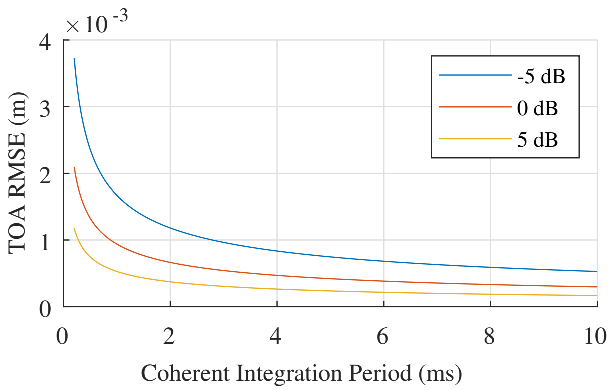

Fig. 4: TOA RMSE bounds for SNRs of -5, 0, and 5 dB over the coherent processing interval.

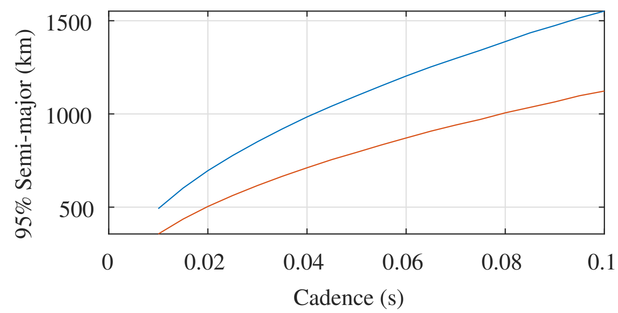

Fig. 5: Semi-major of the error ellipse of solution over the cadence of data bursts for a satellite moving directly overhead (blue), and a satellite reaching at most 70 degrees elevation (orange).

signal. The captured bandwidth of the signal on the UE will be approximately flat. Flat spectra have an effective squared bandwidth of $\gamma^2 = W^2/12$, where in the case of the UE the bandwidth is $W = 2\pi \cdot 25 \cdot 10^6 \approx 157.07 \cdot 10^6$ rad/sec. Varying the coherent integration period, and thus the post integration SNR, will lead to different bounds on the TOA error. This is depicted in Fig. 4 for three pre-correlation SNRs of the signal. Larger data bursts improve accuracy but yield diminishing returns.

B. Data cadence

The cadence at which the RS provides the UE with additional symbols determines the number of measurements the UE has to estimate its position and clock bias. Since the system is dynamic, with the satellites moving, more measurements may smooth out short-term variations in errors, and could help improve the Geometric Dilution of Precision (GDOP) of the solution. The closer measurements are taken, the more correlated they are, and the less unique information they provide. A truly informed decision on the cadence of the data bursts would require a realization of satellite tracks.

The error bounds on the final solution will depend on $P = (H^\mathsf{T} R^{-1} H)^{-1}$, where R is the measurement covariance matrix and H is the measurement matrix. The measurement matrix H can only be formed with some realization of the satellite tracks. Once an error covariance is computed, we can transform the ECEF errors to ENU, and calculate the semi-major axis of the error ellipse. This is depicted in Fig. 5 for a single satellite moving directly overhead, and a satellite reaching at most 70 degrees elevation. The bounds on the error will decrease as more satellites are used in the solution, but the relationship between the data burst cadence and error remains the same.

VI. Ephemeris Error Modeling

At any given epoch, the position of a OneWeb satellite can be retrieved from publicly available TLEs. The accuracy of the satellite position when retrieved from a TLE is typically km-level accurate, with spatial errors reaching 1 to 10 km 24 hours after a TLE file is updated [40]. Spatial ephemeris errors become a source of error in pseudorange measurements. This subsection aims to characterize how the spatial ephemeris error affects the differential pseudorange error when measured at the RS and UE.

Let $\boldsymbol{r}_\mathrm{s}$ denote the true position of the satellite, $\boldsymbol{r}_\mathrm{r}$ denote the known position of the RS, and $\boldsymbol{r}_\mathrm{u}$ be the true position of the UE. The true pseudoranges between $\boldsymbol{r}_\mathrm{r}$ and $\boldsymbol{r}_\mathrm{s}$, and $\boldsymbol{r}_\mathrm{u}$ and $\boldsymbol{r}_\mathrm{s}$, are denoted ρ_r and ρ_u, respectively, are expressed as

$$\rho_\mathrm{r} = \sqrt{(\boldsymbol{r}_\mathrm{r} - \boldsymbol{r}_\mathrm{s})^\mathsf{T}(\boldsymbol{r}_\mathrm{r} - \boldsymbol{r}_\mathrm{s})} \tag{16}$$

$$\rho_\mathrm{u} = \sqrt{(\boldsymbol{r}_\mathrm{u} - \boldsymbol{r}_\mathrm{s})^\mathsf{T}(\boldsymbol{r}_\mathrm{u} - \boldsymbol{r}_\mathrm{s})} \tag{17}$$

Now, suppose that the assumed satellite position contained a 3D spatial error $\boldsymbol{\epsilon}$. The resulting pseudorange when assuming the erroneous satellite position at the RS, $\tilde{\rho}_\mathrm{r}$, and UE, $\tilde{\rho}_\mathrm{u}$, are expressed as

$$\tilde{\rho}_\mathrm{r} = H_\mathrm{r}\boldsymbol{\epsilon} + \rho_\mathrm{r} \tag{18}$$

$$\tilde{\rho}_\mathrm{u} = H_\mathrm{u}\boldsymbol{\epsilon} + \rho_\mathrm{u} \tag{19}$$

where H_r and H_u are the 1×3 Jacobians with respect to the satellites position, expressed as

$$H_\mathrm{r} = \frac{\partial \rho_\mathrm{r}}{\partial \boldsymbol{r}_\mathrm{s}} = -\hat{\boldsymbol{r}}_\mathrm{r} = -\frac{\boldsymbol{r}_\mathrm{r} - \boldsymbol{r}_\mathrm{s}}{\rho_\mathrm{r}} \tag{20}$$

$$H_\mathrm{u} = \frac{\partial \rho_\mathrm{u}}{\partial \boldsymbol{r}_\mathrm{s}} = -\hat{\boldsymbol{r}}_\mathrm{u} = -\frac{\boldsymbol{r}_\mathrm{u} - \boldsymbol{r}_\mathrm{s}}{\rho_\mathrm{u}} \tag{21}$$

The pseudorange measurement error at the RS and the UE due to the spatial error of the satellite will manifest differently due to the different geometry. However, if the positions of the RS and UE are close to each other, the errors will be small. The relative differential pseudorange error between the RS and the UE due to spatial ephemeris error is denoted as η, and is expressed as

$$\begin{aligned}\eta &= (\tilde{\rho}_\mathrm{r} - \rho_\mathrm{r}) - (\tilde{\rho}_\mathrm{u} - \rho_\mathrm{u}) \\ &= (H_\mathrm{r} - H_\mathrm{u})\,\boldsymbol{\epsilon}\end{aligned} \tag{22}$$

For example, consider a specific $\boldsymbol{r}_\mathrm{r}$, $\boldsymbol{r}_\mathrm{u}$, $\boldsymbol{r}_\mathrm{s}$, and 3D satellite spatial error $\boldsymbol{\epsilon} \sim \mathcal{N}(\boldsymbol{0}, P_{\boldsymbol{\epsilon}})$, then

$$\eta \sim \mathcal{N}(0, \sigma_\eta^2) \tag{23}$$

with

$$\sigma_\eta^2 = (H_\mathrm{r} - H_\mathrm{u})\, P_{\boldsymbol{\epsilon}}\, (H_\mathrm{r} - H_\mathrm{u})^\mathsf{T} \tag{24}$$

The distribution of η in (23) requires the knowledge of $\boldsymbol{r}_\text{u}$ to compute the Jacobian which is required for σ_η^2. In practice, $\boldsymbol{r}_\text{u}$ is unknown, but the CT will have *a priori* information about $\boldsymbol{r}_\text{u}$ relative to $\boldsymbol{r}_\text{r}$. For instance, the CT might know that it is located within the same beam footprint as the CS. In this case, $\boldsymbol{r}_\text{u}$ is modeled as

$$\boldsymbol{r}_\text{u} = \boldsymbol{r}_\text{r} + \boldsymbol{\xi} \tag{25}$$

where $\boldsymbol{\xi}$ is a 3D random offset with respect to $\boldsymbol{r}_\text{r}$, following some distribution with covariance $P_{\boldsymbol{\xi}}$. Since $\boldsymbol{r}_\text{u}$ is now treated as a random variable, $H_\text{u}(\boldsymbol{\xi})$ and $\sigma_\eta^2(\boldsymbol{\xi})$ also become random variables. $H_\text{u}(\boldsymbol{\xi})$ is expressed as

$$H_\text{u}(\boldsymbol{\xi}) = H_\text{r} + \boldsymbol{\xi}^\mathsf{T} A \tag{26}$$

with

$$A^\mathsf{T} = \frac{\partial H_\text{r}^\mathsf{T}}{\partial \boldsymbol{r}_\text{r}} = r_\text{r}^{-1}\left(\hat{\boldsymbol{r}}_\text{r}\hat{\boldsymbol{r}}_\text{r}^\mathsf{T} - \mathbb{I}\right) \tag{27}$$

where A is the Jacobian of H_r with respect to $\boldsymbol{r}_\text{r}$. The derivation of this Jacobian can be found in [41]. Consequently, (24) is reduced to

$$\sigma_\eta^2(\boldsymbol{\xi}) = \boldsymbol{\xi}^\mathsf{T} A P_{\boldsymbol{\epsilon}} A^\mathsf{T} \boldsymbol{\xi} \tag{28}$$

Now, $\sigma_\eta^2(\boldsymbol{\xi})$ is a function of the unknown random vector $\boldsymbol{\xi}$, so solving for $\bar{\sigma}_\eta^2$ is required for modeling purposes. Note, (28) is a quadratic form, thus

$$\bar{\sigma}_\eta^2 = \mathbb{E}\left[\sigma_\eta^2(\boldsymbol{\xi})\right] = \text{trace}\left(A P_{\boldsymbol{\epsilon}} A^\mathsf{T} P_{\boldsymbol{\xi}}\right) \tag{29}$$

Finally, the distribution of η when $\boldsymbol{r}_\text{u}$ is unknown can be modeled as

$$\eta \sim \mathcal{N}(0,\, \bar{\sigma}_\eta^2). \tag{30}$$

Consider the scenario where the ephemeris error is zero-mean Gaussian in the ENU frame, with covariance matrix $P_{\boldsymbol{\epsilon}} = \sigma_\text{eph}^2\mathbb{I}$. Also, assume that $\xi \sim \mathcal{N}(\boldsymbol{0}, P_{\boldsymbol{\xi}})$, where $P_{\boldsymbol{\xi}} = \text{diag}\left(\sigma_\text{e}^2, \sigma_\text{n}^2, \sigma_\text{u}^2\right)$, centered at the RS. The choices of σ_eph^2, σ_e^2, σ_n^2, and σ_u^2 are treated as tuning parameters. The values of σ_e^2, σ_n^2, and σ_u^2 depend on the assumed distance between the RS and UE.

In the case of Oneweb, it is required that the RS and UE occupy the same beam footprint. Consider two scenarios: (1) a dense RS network where the UE's position is Gaussian with $P_{\boldsymbol{\xi}} = \text{diag}\left(3300^2, 3300^2, 50^2\right)$ and (2) a sparse RS network where UE's position is Gaussian with $P_{\boldsymbol{\xi}} = \text{diag}\left(25000^2, 25000^2, 1000^2\right)$. Additionally, let $\sigma_\text{eph} = 2.5$ km and assume a typical Oneweb to beam footprint geometry. If a dense RS network is available, the spatial relative pseudorange error between RS and UE can be expected to be small, as $\bar{\sigma}_\eta = 9.0$ m. On the other hand, if a sparse RS network is available, the spatial relative pseudorange error becomes much larger, as $\bar{\sigma}_\eta = 67.8$ m. The distribution of η will be exploited in Section VII.

VII. Estimation

The UE has access to its own TOAs $t_\text{r}(l,m)$, the TOTs $t^*(l,m)$ that have already been compensated from the RS, its own Doppler measurements $f_\text{D}(l,m)$, and the position $\boldsymbol{r}_\text{s}(l,m)$ and velocity $\boldsymbol{v}_\text{s}(l,m)$ of the satellites at the TOT. Given the results in Sec. VI, the UE will not be able to estimate its clock bias in a single variable because each satellite will have a different spatial ephemeris error which will manifest as a different clock bias over a short time duration. As such, for a stationary UE, we must estimate its position $\boldsymbol{r}_\text{u}$, a frame clock offset consisting of the receiver bias and the ephemeris-error pseudorange bias for each satellite $b(s_{l,m}) = \delta t_\text{r} + \eta(s_{l,m})$, a frame clock drift $\dot{\delta t}_\text{r}$, and a carrier clock drift for each satellite $\dot{\delta t}_\text{c}(s_{l,m})$ which is the relative carrier clock drift between the UE and the satellite.

The value $s_{l,m} \in \{0, 1, ..., N_s - 1\}$ is a mapping from beam and frame index to a satellite index for N_s satellites. For example, if two measurements are from the same satellite and the first is from beam i with frame index k, while the second is from beam j with frame index p, they map to the same satellite $s_{i,k} = s_{j,p}$ and have a common clock biases $b(s_{i,k}) = b(s_{j,p})$. For a measurement identified by (l,m), our observables are the pseudorange and the range-rate:

$$\begin{bmatrix}\rho(l,m)\\ \dot{\rho}(l,m)\end{bmatrix} = \begin{bmatrix}c[t_\text{r}(l,m) - t^*(l,m)]\\ -\lambda f_\text{D}(l,m)\end{bmatrix} + \begin{bmatrix}w_\rho(l,m)\\ w_{\dot{\rho}}(l,m)\end{bmatrix} \tag{31}$$

where w_ρ and $w_{\dot{\rho}}$ are both zero-mean Gaussian noise with variances σ_ρ^2 and $\sigma_{\dot{\rho}}^2$.

It is important to note here that $\dot{\rho}(m,l)$ is the carrier clock drift, and not the rate of the pseudoranges obtained from the frame clock $\rho(m,l)$. A measurement vector $\boldsymbol{z}$ is constructed of all the pseudorange measurements followed by all the carrier range-rate measurements.

A. Least squares estimation

Suppose the UE has N_f measurements per beam, from N_b beams corresponding to N_s satellites. There are $N_z = N_\text{f}N_\text{b}$ total pairs of measurements. The state the UE must estimate is

$$\boldsymbol{x} = \begin{bmatrix}\boldsymbol{r}_\text{u}^\mathsf{T} & \boldsymbol{b}^\mathsf{T} & \dot{\delta t}_\text{r} & \dot{\boldsymbol{\delta t}}_\text{c}{}^\mathsf{T}\end{bmatrix}^\mathsf{T} \tag{32}$$

where $\boldsymbol{r}_\text{u} \in \mathbb{R}^3$, $\boldsymbol{b}, \dot{\boldsymbol{\delta t}}_\text{c} \in \mathbb{R}^{N_\text{s}}$, and $\dot{\delta t}_\text{r} \in \mathbb{R}$.

The nonlinear measurement model is

$$\begin{bmatrix}h_\rho(\boldsymbol{x}; l,m)\\ h_{\dot{\rho}}(\boldsymbol{x}; l,m)\end{bmatrix} = \begin{bmatrix}||\boldsymbol{r}(l,m)|| + b(s_{l,m}) + t_\text{r}(l,m)\dot{\delta t}_\text{r}\\ \hat{\boldsymbol{r}}^\mathsf{T}(l,m)\boldsymbol{v}_\text{s}(l,m) + \dot{\delta t}_\text{c}(s_{l,m})\end{bmatrix} \tag{33}$$

where $\boldsymbol{r}(l,m)$ is the vector pointing from satellite $s_{l,m}$ to the rover, and $\hat{\boldsymbol{r}}(l,m)$ is its unit vector. All measurements are in meters and meters per second.

Let H be the linearized measurement model

$$\begin{aligned} H_\rho &= \begin{bmatrix}\frac{\partial h_\rho(\boldsymbol{x};0,0)}{\partial \boldsymbol{x}} & \dots & \frac{\partial h_\rho(\boldsymbol{x};N_\text{b}-1,N_\text{f}-1)}{\partial \boldsymbol{x}}\end{bmatrix}^\mathsf{T} \\ H_{\dot{\rho}} &= \begin{bmatrix}\frac{\partial h_{\dot{\rho}}(\boldsymbol{x};l,m)}{\partial \boldsymbol{x}} & \dots & \frac{\partial h_{\dot{\rho}}(\boldsymbol{x};N_\text{b}-1,N_\text{f}-1)}{\partial \boldsymbol{x}}\end{bmatrix}^\mathsf{T} \\ H &= \begin{bmatrix}H_\rho\\ H_{\dot{\rho}}\end{bmatrix} \end{aligned} \tag{34}$$

With the linearized measurement model, an increment from the current estimate $\Delta\boldsymbol{x}$ can be calculated and used to update the estimate $\hat{x} + \Delta\boldsymbol{x}$, repeating for as many iterations as desired.

B. Altitude Constraint

The estimator includes an altitude constraint by employing a Gaussian distributed pseudo-measurement parameterized by a mean μ_{alt} and variance σ^2_{alt} of the altitude with respect to the WGS-84 ellipsoid. This pseudo-measurement constrains the altitude of the UE and allows us to keep position in the ECEF coordinate system instead of converting at each step to a geodetic coordinate system. To apply the constraint, we can add a term to the measurements and extend the measurement model similar to [11]:

$$z_{2N_z+1} = \mu_{\text{alt}} \tag{35}$$

$$h_{\text{alt}}(\boldsymbol{x}) = \texttt{alt}(\boldsymbol{r}_{\text{u}})$$

$$H_{2N_z+1} = \left[\cos(\phi_{\text{lat}})\cos(\lambda_{\text{lon}}), \cos(\phi_{\text{lat}})\sin(\lambda_{\text{lon}}), \sin(\phi_{\text{lat}}), 0\right] \tag{36}$$

where $\texttt{alt}(\boldsymbol{r}_{\text{u}})$ returns the altitude of $\boldsymbol{r}_{\text{u}}$ with respect to the WGS-84 ellipsoid, ϕ_{lat} and λ_{lon} are the latitude and longitude of $\boldsymbol{r}_{\text{u}}$, respectively. The measurement covariance matrix R is also augmented with an additional element on the diagonal, σ^2_{alt} that is independent from all other measurements.

C. Frame Clock bias constraint

As shown in (33), the pseudorange measurements from satellite $s_{l,m}$ contain a constant measurement bias $b(s_{l,m}) = \delta t_r + \eta(s_{l,m})$, where $\eta(s_{l,m})$ is an additional bias term due to the spatial ephemeris error of satellite $s_{l,m}$. As the UE gets pseudorange measurements from a new satellite $s_{i,k}$, there will be an instantaneous jump in pseudorange bias due to the new $\eta(s_{i,k})$. Rather than estimating each $b(s_{l,m})$ independently, the UE can exploit the distribution of $\eta(s_{l,m})$ to constrain the estimate of $b(s_{l,m})$ for $s_{l,m} = 1, 2, ..., N_s - 1$ with respect to $b(0)$. This can be accomplished via $N_s - 1$ pseudo-measurements, where each pseudo-measurement is the difference between $b(s_{l,m})$ and $b(0)$ for $s_{l,m} = 1, 2, ..., N_s - 1$. The Jacobian H_{b} and its corresponding measurement covariance matrix R_{b} becomes

$$H_{\text{b}} = \left[\mathbf{0}_{N_s-1\times 3}, \mathbf{1}_{N_s-1\times 1}, -\mathbb{I}_{N_s-1\times N_s-1}, \mathbf{0}_{N-1\times N+1}\right] \tag{37}$$

$$R_{\text{b}} = \text{diag}\left(\bar{\sigma}^2_\eta(1), \bar{\sigma}^2_\eta(2), ..., \bar{\sigma}^2_\eta(N_s - 1)\right) + \bar{\sigma}^2_\eta(0)\mathbf{1}_{N_s-1\times N_s-1} \tag{38}$$

This set of $N_s - 1$ pseudo-measurements are independent of the other measurements, but have a common covariance due to $\eta(0)$. The values of $\bar{\sigma}_\eta(s_{i,k})$ are calculated for each satellite, given the satellite's position and the *a priori* information of $\boldsymbol{r}_{\text{u}}$ with respect to $\boldsymbol{r}_{\text{r}}$. As the UE gets farther away from the RS, the constraint on the bias becomes weaker. If the UE does not have *a priori* information of $\boldsymbol{r}_{\text{u}}$ with respect to $\boldsymbol{r}_{\text{r}}$, this will result in estimating each $b(s_{l,m})$ independently. However, this is an unlikely scenario because the UE will need to know which RS to retrieve timing corrections from. This constraint on $\boldsymbol{b}$ significantly improves observability, resulting in a smaller error ellipse.

VIII. Results

Our field experiment consisted of a single RS located on the campus of The University of Texas at Austin, and a single UE located roughly 3 km Northeast of the RS. Both the RS and UE were centered to capture at 11.575 GHz, or channel 4 from [20]. This section presents the results of the experiment given the advocated framework in this paper.

A. RS hardware and capabilities

The RS is equipped with a steerable 90-cm offset parabolic dish with an approximately 3-degree beamwidth. Using publicly available ephemerides from NORAD in the form of TLEs, we can steer the dish to track OneWeb satellites overhead. Our antenna's beamwidth limits captures to a single satellite at a time, which for OneWeb's fixed beam approach is sufficient.

Fig. 6 outlines the hardware used to capture the raw IQ samples. Our parabolic dish is equipped with a feedhorn connected to a low-noise block (LNB) with a conversion gain of 60 dB and a noise figure of 0.8 dB. The LNB downconverts 10.7–11.7 GHz signals to 950–1950 MHz, or 11.7–12.75 GHz to 1100–2150 MHz. The antenna's nominal gain is 40 dBi at 12.5 GHz, with at least 4-5 dB of losses due to lack of circular-to-linear polarizer and feedhorn misalignment. The antenna is located on the campus of the University of Texas at Austin, with a clear view of the sky.

The downstream hardware performs additional downmixing, bandpass filtering, and 16-bit complex sampling. Both the LNB and downstream downconversion and sampling hardware are locked to the same GPS-disciplined oven-controlled crystal oscillator (OCXO).

The usable bandwidth of the capture is 200 MHz. The capture system is capable of capturing on two channels at once, with the limitation that the sampling rate must be identical for the sampling to begin simultaneously. Alongside the OneWeb captures, we simultaneously capture GPS centered at L1 to obtain a true time of arrival for the OneWeb signal at the RS. While our capturing equipment is capable of continuous capture, we opted for 70-second captures due to storage limitations. The 70 seconds are enough for clear captures of three to four beams per satellite.

For OneWeb, the RS must be able to capture the entire signal's bandwidth to decode it, since it is a SC signal. This offers a good point of comparison with an OFDM-based signal like Starlink, since a RS under the same framework for Starlink could make do with some subset of the bandwidth, and in fact wouldn't gain much from capturing at a wider bandwidth than the UE. A high gain antenna on the RS is key, since the higher the received SNR the less bit error rate (BER) the RS will have after decoding, maximizing the correlation on the UE side.

B. UE Setup

Our UE is equipped with a Ku-band feedhorn pointing towards zenith. The feedhorn is connected to an LNB identical

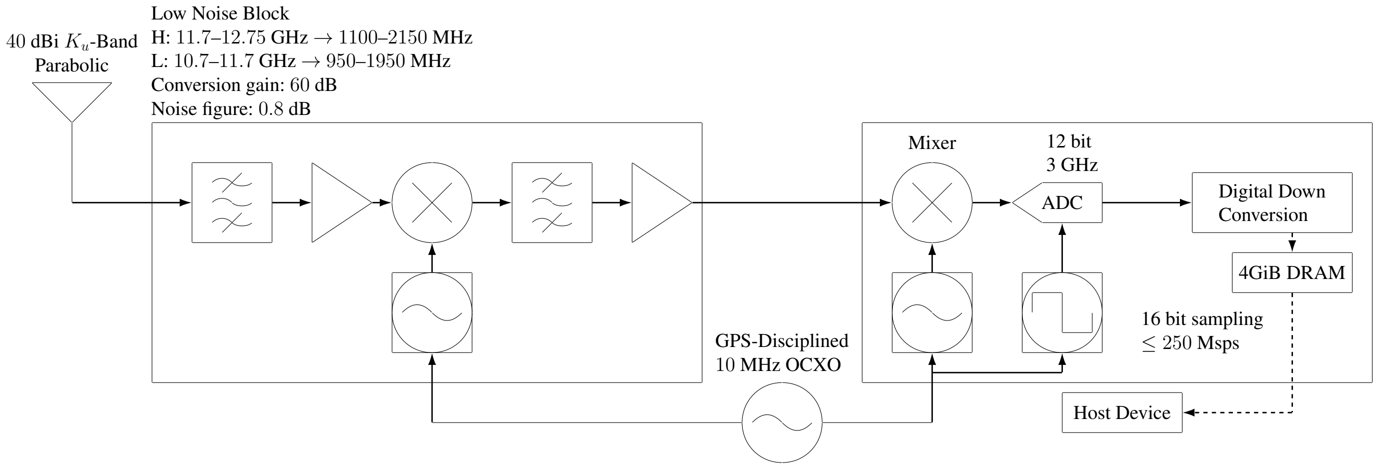

Fig. 6: Block diagram of the OneWeb signal capture process at the RS.

to the one at the RS. The hardware performs downmixing to baseband, bandpass filtering, and 16-bit complex sampling. Both the downmixing in the LNB and in the sampling operations in the downstream hardware are phase-locked to a common GPS-disciplined OCXO to minimize the effects of receiver clock variations. The capture system is also capable of capturing on two channels at once. We take advantage of this dual capture process to simultaneously capture GPS centered at L1 for truth data. Both channels capture at 25 Msps. On the UE, we capture continuously for around 30 minutes to maintain coherence between the captures of the satellite beams.

We had initially planned on estimating only a single frame clock offset for the entire capture. As mentioned in Sec. VII-C, the different errors from each TLE manifested as different frame clock biases per satellite, rendering the problem infeasible to solve without estimating the biases separately. In a more realistic scenario, the RS may have access to ephemerides of better quality than TLEs. Alternatively, if a network of RS are used with visibility of the same satellites, the RS network could estimate its own corrections to the ephemerides.

Unlike the RS, the UE need not have a large gain antenna, or even a large bandwidth since no decoding occurs on the UE. These factors enable a cheaper and more portable UE. Our realization of the UE relies on GPS-disciplining to keep the clock drift low. Since the RS doesn't continuously capture, and the gaps in the captures while repositioning to a new satellite are large, long idle periods would result in a poor-quality clock to drift without measurements to correct it. In practice, where both RS and UE would be continuously capturing, the UE could forgo the GPS-disciplining. Additionally, the RS could capture on multiple channels, allowing the UE to switch between them to minimize the gaps between beams.

C. Experimental Results

As a satellite moves overhead, and its signal is captured by both the RS and UE, the RS begins decoding the frames as they come in. This process is identical to the one outlined in [20]. For each frame, the RS also obtains the TOT as outlined in Sec. IV-C. For our experiment, we opted to provide the UE with 2 ms of data every 50 ms which, if done in real time would require a link capable of 2.304 MB/s on average. Compared to the data required to be sent over per frame, the data burden for clock and orbital corrections in the form of TOTs and satellite positions and velocities are negligible.

On the other end the UE uses the received partial payload data to generate a local replica with which to correlate the incoming signal against. For our experiment we used the BLS process outlined in Sec. VII in post-processing. In practice this would be replaced by a sequential estimator that would use new TOAs to update the current state estimate as they come in. The TOAs along with the reference-provided TOTs are used to estimate the position and clock error of the UE.

Our data was collected over roughly a 30-minute period in January 2025. The captures consisted of 12 satellites, the ground-tracks of which are shown in Fig. 7. We ran the BLS process once to obtain the standard deviation of the residuals. Using twice the standard deviation of the first run in our noise covariance matrix, we ran the BLS process again to obtain our solution. For each satellite, the standard deviation of the noise provided for the pseudoranges was between 3.3 and 4.1 m, and for the Doppler measurements between 0.2 and 0.9 m/s. The residuals from the second run are shown in Fig. 8, and the final position estimate is shown in Fig. 9.

The bias constrains from Sec. VII-C were calculated to assume that the UE's position was Gaussian-distributed with $\sigma_e = \sigma_n = 3.3$ km and $\sigma_u = 50$ m around the RS. The TLE's were 12 hours old, so $\sigma_{\text{eph}} = 2.5$ km was used. The BLS process was robust enough where even initializing the position estimate 250 km away from the true position, the solution converged to the same point. The final position estimate was within 0.35 m of the true position, with the solution contained within a 95% error ellipse with a semi-major of 36.38 m and a semi-minor of 2.40 m. Importantly, timing was resolved to within about 69.49 ns with 95% confidence.When assuming a sparse RS network, the UE's position was modeled as Gaussian distributed with $\sigma_e = \sigma_n = 25$ km and $\sigma_u = 1$ km around the RS, resulting in the semi-minor growing to 15.17 m. The results show that the framework outlined in this paper is feasible and can provide accurate position estimates,

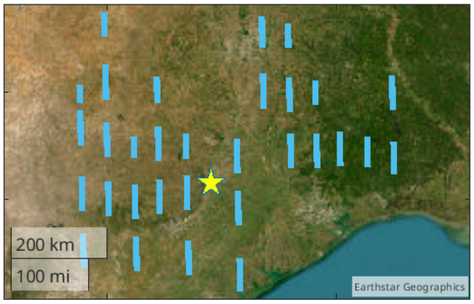

Fig. 7: The track each of the 12 satellites took, projected on the Earth, only while their beams were active.

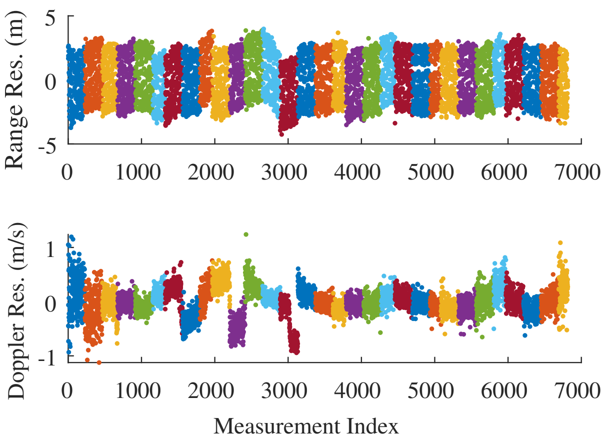

Fig. 8: Pseudorange (top) and Doppler (bottom) residuals from the BLS process for 6815 measurements of 12 satellites, with 1-4 beams captured per satellite, spanning about 30 minutes.

along with clock bias and bias rate estimates.

Future work will focus extending this work by reducing some sources of error in the process described so far. A sub-sample super-resolution method to obtain TOA and Doppler measurements would significantly reduce the measurement noise. Additionally, while the pseudorange measurements on the UE benefited from RS corrections, the range-rate measurements were not corrected. Jumps in the range-rate measurements in Fig. 8 are due to carrier clock jumps from the satellites and remained unmodeled in the BLS process.

IX. Conclusions

With this paper we outline a framework for a pseudorange-based PNT solution using OneWeb's downlink signal and the cooperation of a third-party providing timing corrections and data aiding to extend the coherent integration period. Further, we demonstrate through an experiment the feasibility of the proposed framework. Given the additional challenges our experimental setup faced compared to a real-world scenario, we believe the framework and our results show that using broadband communications signals from LEO for PNT is competitive with traditional GNSS. If implemented correctly, it could provide better timing and positioning services than traditional GNSS.

Fig. 9: Final UE position estimate, with the true position indicated with a star. The error of the final estimate is 0.35m, with the solution contained within a 95% error ellipse, which has a semi-major of 36.38m and a semi-minor of 2.40m.

Acknowledgments

Research was supported by the U.S. Department of Transportation under Grant 69A3552348327 for the CARMEN+ University Transportation Center, and by affiliates of the 6G@UT center within the Wireless Networking and Communications Group at The University of Texas at Austin.

References

[1] P. A. Iannucci and T. E. Humphreys, "Fused low-Earth-orbit GNSS," *IEEE Transactions on Aerospace and Electronic Systems*, pp. 1–1, 2022.

[2] N. Jardak and Q. Jault, "The potential of LEO satellite-based opportunistic navigation for high dynamic applications," *Sensors*, vol. 22, no. 7, p. 2541, 2022.

[3] Z. Kassas, in *Navigation from low earth orbit — Part 2: Models, implementation, and performance in Position, Navigation, and Timing Technologies in the 21st Century*, 2021, vol. 2.

[4] M. L. Psiaki, "Navigation using carrier Doppler shift from a LEO constellation: TRANSIT on steroids," *NAVIGATION*, vol. 68, no. 3, pp. 621–641, 2021.

[5] T. E. Humphreys, P. A. Iannucci, Z. M. Komodromos, and A. M. Graff, "Signal structure of the Starlink Ku-band downlink," *IEEE Transactions on Aerospace and Electronic Systems*, pp. 1–16, 2023.

[6] A. M. Graff and T. E. Humphreys, "OFDM-based positioning with unknown data payloads: Bounds and applications to LEO PNT," *IEEE Transactions on Wireless Communications*, 2024, submitted for review.

[7] T. E. Humphreys, "Interference," in *Springer Handbook of Global Navigation Satellite Systems*. Springer International Publishing, 2017, pp. 469–503.

[8] M. J. Murrian, L. Narula, P. A. Iannucci, S. Budzien, B. W. O'Hanlon, M. L. Psiaki, and T. E. Humphreys, "First results from three years of GNSS interference monitoring from low Earth orbit," *NAVIGATION*, vol. 68, no. 4, pp. 673–685, 2021.

[9] Z. Clements, P. Ellis, and T. E. Humphreys, "Dual-satellite geolocation of terrestrial GNSS jammers from low Earth orbit," in *Proceedings of the IEEE/ION PLANS Meeting*, Monterey, CA, 2023, pp. 458–469.

[10] G. S. Workgroup, "GPS spoofing: Final report of the GPS spoofing workgroup," OPSGROUP, Tech. Rep., 2024. [Online]. Available: https://ops.group/blog/gps-spoofing-final-report

[11] Z. L. Clements, P. B. Ellis, M. J. Murrian, M. L. Psiaki, and T. E. Humphreys, "Single-satellite-based geolocation of broadcast GNSS spoofers from low Earth orbit," *NAVIGATION*, 2025, submitted for review.

[12] W. S. Limited, "Amendment to modification application for U.S. Market Access Grant for the OneWeb Ku- and Ka-Band system," https://licensing.fcc.gov/myibfs/download.do?attachment_key=3495551, Jan. 2021, SAT-APL-20210112-00007.

[13] H. Sallouha, S. Saleh, S. De Bast, Z. Cui, S. Pollin, and H. Wymeersch, “On the ground and in the sky: A tutorial on radio localization in ground-air-space networks,” *IEEE Communications Surveys and Tutorials*, vol. 27, no. 1, pp. 218–258, 2025.

[14] B. McLemore and M. L. Psiaki, “Navigation using Doppler shift from LEO constellations and INS data,” *IEEE Transactions on Aerospace and Electronic Systems*, vol. 58, no. 5, pp. 4295–4314, 2022.

[15] A. Baron, P. Gurfil, and H. Rotstein, “Implementation and accuracy of Doppler navigation with LEO satellites,” *NAVIGATION: Journal of the Institute of Navigation*, vol. 71, no. 2, 2024.

[16] T. Fan, T. Zhang, H. Zhang, J. Mo, and X. Niu, “A double sideband combined tracking method for Galileo E5 AltBOC signals,” *Satellite Navigation*, vol. 4, no. 1, p. 27, 2023.

[17] W. Qin, Z. M. Komodromos, and T. E. Humphreys, “An analysis of the short-term time stability of the Starlink Ku-band downlink frame clock,” in *Proceedings of the IEEE International Conference on Wireless for Space and Extreme Environments (WISEE 2024)*, 2024.

[18] W. Qin, A. M. Graff, Z. L. Clements, Z. M. Komodromos, and T. E. Humphreys, “Timing properties of the Starlink Ku-band downlink,” *IEEE Transactions on Aerospace and Electronic Systems*, 2025, submitted for review.

[19] E. Rubinov, “FrontierSI State of the Market Report LEO PNT 2024 Edition,” Jan. 2025, https://frontiersi.com.au/wp-content/uploads/2025/01/FrontierSI-State-of-Market-Report-LEO-PNT-2024-Edition-v1.1.pdf.

[20] Z. M. Komodromos, Z. L. Clements, and T. E. Humphreys, “Signal parameter estimation and demodulation of the OneWeb Ku-Band downlink,” *IEEE Transactions on Aerospace and Electronic Systems*, 2025, in preparation.

[21] W. Van Uytsel, T. Janssen, M. Weyn, and R. Berkvens, “A technical overview of current “new space” LEO-PNT initiatives and their application potential,” in *2024 IEEE 35th International Symposium on Personal, Indoor and Mobile Radio Communications (PIMRC)*. IEEE, 2024, pp. 1–6.

[22] N. S. Miller, J. T. Koza, S. C. Morgan, S. M. Martin, A. Neish, R. Grayson, and T. Reid, “SNAP: A Xona Space Systems and GPS software-defined receiver,” in *2023 IEEE/ION Position, Location and Navigation Symposium (PLANS)*. IEEE, 2023, pp. 897–904.

[23] P. A. Iannucci and T. E. Humphreys, “Economical fused LEO GNSS,” in *Proceedings of the IEEE/ION PLANS Meeting*, 2020.

[24] A. M. Graff and T. E. Humphreys, “Ziv-Zakai-optimal OFDM resource alocation for time-of-arrival estimation,” *IEEE Transactions on Wireless Communications*, 2025.

[25] Z. M. Kassas, N. Khairallah, and S. Kozhaya, “Ad astra: Simultaneous tracking and navigation with megaconstellation LEO satellites,” *IEEE Aerospace and Electronic Systems Magazine*, 2024.

[26] S. Shahcheraghi, J. Saroufim, and Z. M. Kassas, “Acquisition, Doppler tracking, and differential LEO-aided IMU navigation with uncooperative satellites,” *IEEE Transactions on Aerospace and Electronic Systems*, 2025.

[27] J. Saroufim and Z. M. Kassas, “Ephemeris and timing error disambiguation enabling precise LEO PNT,” *IEEE Transactions on Aerospace and Electronic Systems*, 2025.

[28] S. Zhou, R. Yang, Y. Li, X. Zhan, and H. Qin, “Iridium TOA estimation and positioning based on carrier tracking and beam decoding,” *IEEE Transactions on Instrumentation and Measurement*, vol. 74, pp. 1–23, 2025.

[29] S. C. Morgan, Z. M. Komodromos, W. Qin, Z. L. Clements, A. M. Graff, W. J. Morrison, and T. E. Humphreys, “A mock implementation of fused LEO GNSS,” in *Proceedings of the IEEE/ION PLANS Meeting*, Salt Lake City, UT, 2025.

[30] Z. Tan, H. Qin, L. Cong, and C. Zhao, “Positioning using IRIDIUM satellite signals of opportunity in weak signal environment,” *Electronics*, vol. 9, no. 1, p. 37, 2019.

[31] M. Neinavaie, J. Khalife, and Z. M. Kassas, “Acquisition, Doppler tracking, and positioning with Starlink LEO satellites: First results,” *IEEE Transactions on Aerospace and Electronic Systems*, vol. 58, no. 3, pp. 2606–2610, 2022.

[32] N. Jardak, R. Adam, and Q. Jault, “Leveraging multi-LEO satellite signals for opportunistic positioning,” *IEEE Access*, 2024.

[33] D. Odijk and L. Wanninger, “Differential positioning,” in *Springer Handbook of Global Navigation Satellite Systems*. Springer International Publishing, 2017, pp. 753–780.

[34] Radio Communications & EMC, “OneWeb ow70l UT test report FCC id xxz-intow70ldac,” https://fcc.report/FCC-ID/XXZ-INTOW70LDAC/5364479.pdf, 2021, XXZ-INTOW70LDAC.

[35] J. Saastamoinen, “Atmospheric correction for the troposphere and stratosphere in radio ranging of satellites,” in *Geophysical Monograph 15*, S. W. Henriksen, Ed. Washington, D.C.: American Geophysical Union, 1972, pp. 247–251.

[36] A. E. Niell, “Global mapping functions for the atmosphere delay at radio wavelengths,” *Journal of Geophysical Research*, vol. 101, pp. 3227–3246, 1996.

[37] S. Stein, “Algorithms for ambiguity function processing,” *IEEE Transactions on Acoustics, Speech and Signal Processing*, vol. 29, no. 3, pp. 588–599, June 1981.

[38] J. A. Nanzer, M. D. Sharp, and D. Richard Brown, “Bandpass signal design for passive time delay estimation,” in *2016 50th Asilomar Conference on Signals, Systems and Computers*, Nov. 2016, pp. 1086–1091.

[39] M. Skolnik, *Introduction to radar systems 2nd Edition*. McGraw-Hill, 1980.

[40] J. R. Vetter, “Fifty years of orbit determination,” *Johns Hopkins APL technical digest*, vol. 27, no. 3, p. 239, 2007.

[41] Z. Clements, P. Ellis, M. L. Psiaki, and T. E. Humphreys, “Geolocation of terrestrial GNSS spoofing signals from low Earth orbit,” in *Proceedings of the ION GNSS+ Meeting*, Denver, CO, 2022, pp. 3418–3431.